EUROFUSION WPJET1-PR(15) 14380

IM Nunes et al.

Plasma Confinement at JET

Preprint of Paper to be submitted for publication in
Plasma Physics and Controlled Fusion

This work has been carried out within the framework of the EUROfusion Consortium and has received funding from the Euratom research and training programme 2014-2018 under grant agreement No 633053. The views and opinions expressed herein do not necessarily reflect those of the European Commission.

Plasma confinement at JET

I Nunes[1] on behalf of the JET contributors[*]

EUROfusion Consortium, JET, Culham Science Centre, OX14 3DB, Abingdon, UK,
[1]Instituto de Plasmas e Fusão Nuclear, IST, Universidade de Lisboa, Portugal,

e-mail: isabel.nunes@ipfn.tecnico.ulisboa.pt

Abstract. Operation with a Be/W wall at JET (JET-ILW) has an impact on scenario development and energy confinement with respect to the carbon wall (JET-C). The main differences observed were (1) strong accumulation of W in the plasma core and (2) the need to mitigate the divertor target temperature to avoid W sputtering by Be and other low Z impurities and (3) a decrease of plasma energy confinement. A major difference is observed on the pedestal pressure, namely a reduction of the pedestal temperature which, due to profile stiffness the plasma core temperature is also reduced leading to a degradation of the global confinement. This effect is more pronounced in low β_N scenarios. At high β_N, the impact of the wall on the plasma energy confinement is mitigated by the weaker plasma energy degradation with power relative to the IPB98(y,2) scaling calculated empirically for a CFC first wall. The smaller tolerable impurity concentration for tungsten ($<10^{-5}$) compared to that of carbon requires the use of electron heating methods to prevent W accumulation in the plasma core region as well as gas puffing to avoid W entering the plasma core by ELM flushing and reduction of the W source by decreasing the target temperature. W source and the target temperature can also be controlled by impurity seeding. Nitrogen and Neon have been used and with both gases the reduction of the W source and the target temperature is observed. Whilst more experiments with Neon are necessary to assess its impact on energy confinement, a partial increase of plasma energy confinement is observed with Nitrogen, through the increase of edge temperature. The challenge for scenario development at JET is to extend the pulse length curtailed by its transient behavior (W accumulation or MHD), but more importantly by the divertor target temperature limits. Re-optimisation of the scenarios to mitigate the effect of the change of wall materials maintaining high global energy confinement similar to JET-C is underway and JET has successfully achieved $H_{98(y,2)} = 1$ for plasma currents up to 2.5MA at moderate β_N.

1. Introduction and background

The main goal for changing the wall material at JET from carbon fiber composite (CFC) to beryllium (Be) in the main chamber and tungsten (W) or W coated CFC in the divertor was primarily to investigate: material erosion and power handling capability at high plasma performance related with the lifetime of the first wall components and long-term tritium retention related with plant safety of a fusion reactor. Tungsten has high threshold energy for chemical sputtering by hydrogen isotopes leading to low erosion rates and a high temperature threshold for melting compatible with operation of high performance plasmas [1]. As for the main chamber, since erosion is not a big issue in present tokamaks or even in ITER, a low-Z

[*]*See the Appendix of F. Romanelli et al., Proceedings of the 25th IAEA Fusion Energy Conference 2014, Saint Petersburg, Russia*

material was chosen which has the benefit of low radiation with small impact on the plasma behaviour.

The extrapolation of long-term fuel retention based on CFC machines showed unacceptably high values for a fusion reactor whilst it predicted that fueling retention on metallic PFCs should reduce by an order of magnitude relative to all carbon PFCs [2]. After the conversion from all CFC to Be/W PFCs, JET focused its initial programme on the characterization of short- and long-term fuel retention studies. A global gas balance analysis was performed, by using a series of repetitive discharges for low and high triangularity configurations (δ=0.2 and 0.4) at different confinement regimes (ohmic, L-mode and H-mode) with varying levels of deuterium fuelling at a wall temperature of 200ºC. For the ILW, this analysis also includes the variation of the pumping rates, achieved by switching off/on the divertor cryopumps, the turbo pumps and the NBI cryopumps, for the JET-C analysis all the pumping systems are switched on. The results, showed in figure 1 [3], confirmed that the long-term retention for deuterium gas is reduced by a factor of 10-20. The retention rate (D/s) is here defined as the number of retained deuterium ions in the first wall components, determined by the difference between the total injected deuterium gas and the pumped deuterium gas, normalised to the integrated plasma time in divertor configuration where the main ion flux interaction with the PFCs is observed.

The residual content of carbon in the main chamber plasma edge is also reduced by at least a factor of 20 [4] and the power radiation in the divertor is now as low as ~20% and the effective ion charge (Z_{eff}) is ~1.2 (~2 in JET-C) favouring high performance plasmas where performance is here quantified in terms of plasma stored energy, W_{th} and energy confinement time, $\tau_E = W_{th}/P_{heat}$. Operation with high-Z materials is non-trivial [5, 6] mostly due to the high radiation losses in the plasma core caused by the accumulation of W released from sputtering by low-Z impurities, in the JET case, mainly Be.

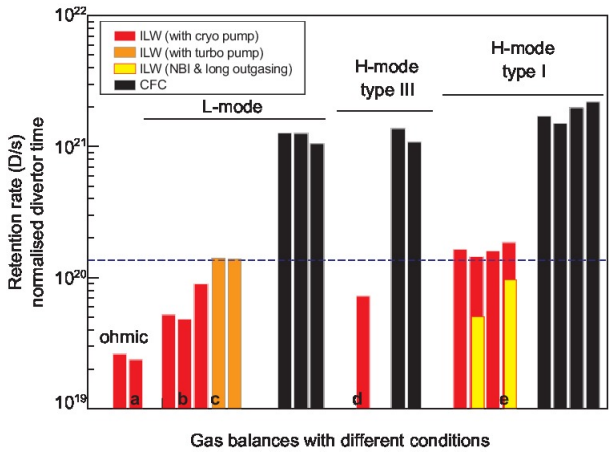

Figure 1 – Comparison of long term outgassing for different plasmas and confinement conditions for JET-C and JET-ILW. Figure from [3].

At JET a small concentration of W in the plasma (<10^{-4}) [7] leads to a slow increase of core radiation resulting in unstable and highly disruptive plasmas. This behaviour is depicted in figure 2(a), which shows the time traces of a typical H-mode where the core plasma temperature is decreasing as the W concentration in the core increases. The increase of the core radiation reduces the core temperature as shown in figure 2(b) and ultimately the plasma suffers a radiative collapse. Reliable operation can be recovered with high-levels of gas puffing. For high energy plasmas, additional core heating is also needed to control the W concentration in the core. As known from the JET-C experiments, plasmas with high gas puffing rate will have reduced plasma performance, mostly due to the loss of the pedestal temperature, which through stiffness reduces the core temperature. Plasma performance is recovered for conditions of optimum pumping, where the neutral pressure at the divertor is reduced and at high normalised plasma pressure (β_N) [8, 9, 10].

This paper is organised as follows: section 2 addresses the methods to control W source and W concentration and its impact on plasma energy confinement. In section 3, a general

overview of the global plasma confinement comparing results from the JET-C era with the JET-ILW era is presented, as well as the most significant changes to the operational space. Sections 4 and 5 describe the changes to the pedestal and core behaviour with the new ITER-like wall. Finally, in section 6 a summary and future plans are described.

2. Controlling W source and W concentration

The W content in the plasma is largely determined by its transport at the edge and in the core. Whilst low particle confinement regimes show a slow increase of W in the core due to their poor confinement, high particle confinement regimes often show a strong increase of W in the core. Peaked density profiles and strong inward particle pinch characteristic of neo-classical transport leads to the accumulation of W in the core and consequently to the decrease of the plasma core temperature reducing the global energy confinement. Ultimately, the temperature profiles can become hollow and a radiative collapse of the plasma is observed. The presence of W in the plasma core can be controlled by: (a) increasing the transport of W from the core to the plasma edge, (b) reducing (screening) the influx of W to the plasma core and (c) reducing the W source i.e., reducing the W sputtering from the divertor by reducing the plasma temperature at the target.

Central electron heating has been successfully used at ASDEX-Upgrade and JET to control W accumulation. In ASDEX-Upgrade, Electron Cyclotron Resonance Heating (ECRH) is routinely used [5], whilst at JET, Ion Cyclotron Resonance Heating (ICRH) is used [11]. Both schemes aim at increasing the plasma core electron temperature. At JET, the effect of ICRH can be described by changes in (a) higher temperature gradients, (b) temperature screening, (c) change in minority temperature and (d) its anisotropy and (e) changes in the electron turbulence. At high density plasmas where the ions are strongly coupled to the electrons, the increase of the ion temperature gradient leads to the increase of temperature screening reducing the W in the core. This behaviour is explained by neo-

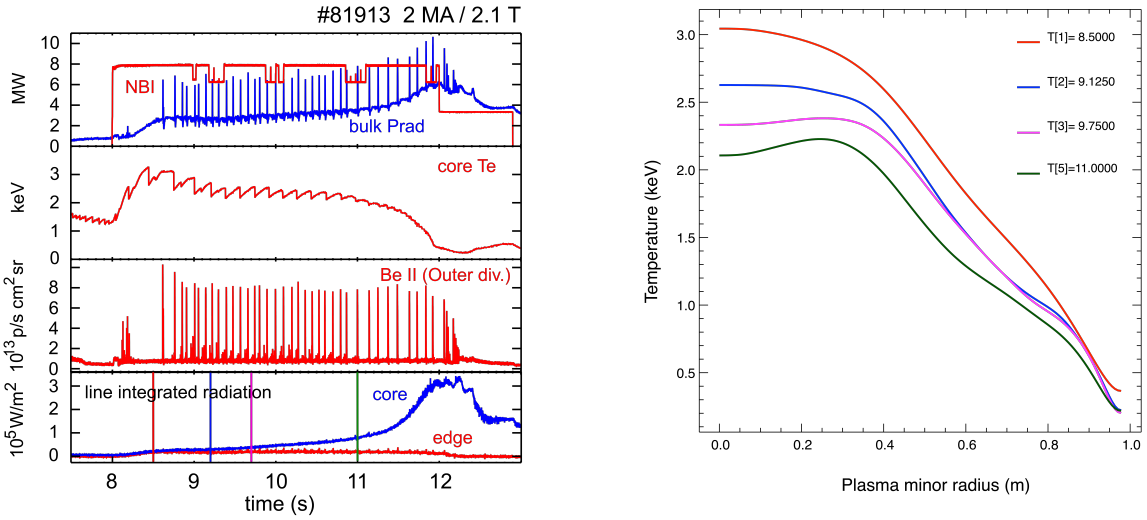

Figure 2 – (a) Typical H-mode plasmas where W accumulation in the core plasma is observed and (b) temperature profiles for different time slices as marked in figure 2(a).

classical effects where the inward particle pinch of high-Z impurities is reduced by the appearance of electron trapped modes (TEM) which cause an outward particle flux leading to the flattening of the density profiles and consequently to the reduction of the W concentration [12, 13]. For the low density plasmas where the ions are decoupled from the electrons, the screening of W is also done by the temperature but here caused by the minority fast ion distribution, enhanced by the anisotropy of the minority heating [14]. The modelling of W transport including impurity poloidal asymmetries and plasma rotation shows good agreement

with experimental results, when both turbulent and neoclassical transport are considered together, since the profile is often set by the ratio of neoclassical convection to turbulent diffusion [15, 16, 17]. Figure 3 shows a comparison between two similar plasmas with neutral beam injection (NBI) only and with NBI plus ICRH. The control of W accumulation with ICRH is strongly correlated with the temperature profile peaking and it is only achievable for ICRH powers (or T_e peaking) above a certain value [11]. Although ICRH is essential to control the W accumulation in the core, it is not sufficient to achieve stationary discharges. A minimum ELM (edge-localised modes) frequency ($f_{ELM} \gtrsim 30\text{Hz}$) for W flushing is necessary, which is achieved in JET by gas puffing.

Flushing of W at the plasma edge by ELMs is very effective in preventing W to reach the

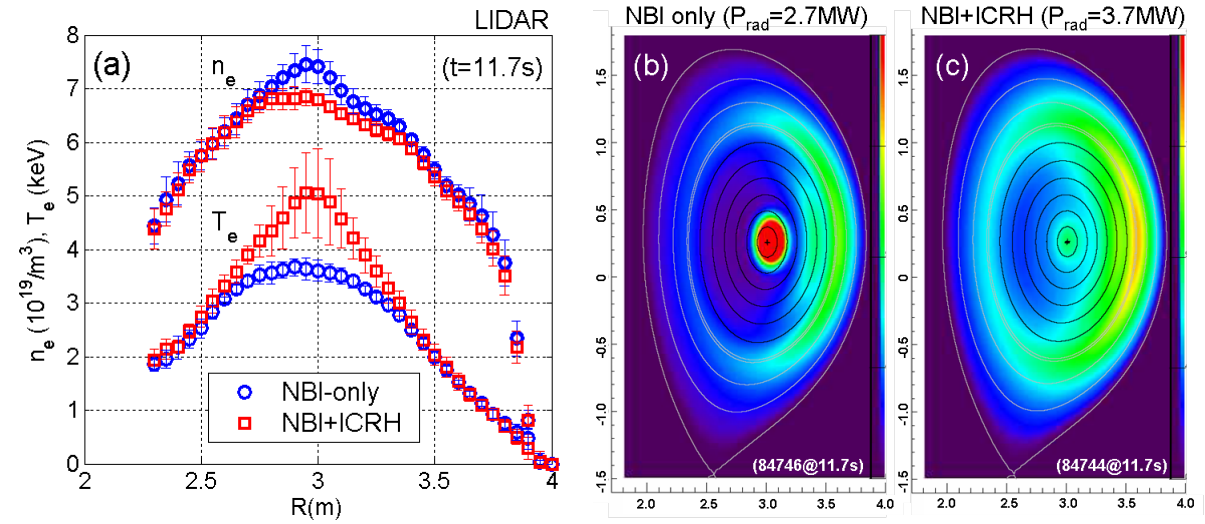

Figure 3 – W accumulation control by means of ICRH. (a) Temperature and density profiles for two similar plasmas with NBI heating only (blue) and NBI+ICRH heating (red). (b) and (c) Tomographic reconstruction of soft X-ray signals for both plasmas showing the radiation distribution due to W. Figures from [11]

core plasma. On the other hand, ELMs contribute to the W source, as these produce large rapid heat fluxes to the divertor causing W sputtering. To achieve an ELM frequency high enough to keep the W penetration low, and reduce the large heat flux to the divertor, gas puffing at rates above 10^{22} Ds^{-1} are used, but as in JET-C, a degradation of energy confinement is observed [18, 19]. Figure 4 shows the time traces for two similar pulses with different rates of gas puffing; $\Gamma_D = 1.54 \cdot 10^{22}$ ele/s for pulse #86586 (red) and $\Gamma_D = 4.02 \cdot 10^{22}$ ele/s for pulse #86587 (blue). The time traces depicted in figure 4 are, from top to bottom: (a) the additional heating power from NBI and ICRH, (b) the radiated bulk power (used here as proxy to the W concentration in the plasma core) (c) gas puffing rate, (d) plasma stored energy and (e-f) the D_α traces as a proxy for the ELM frequency. The bulk radiation is measured using either the vertical or horizontal bolometer channels viewing half of the plasma volume excluding the divertor region. In both cases it is assumed toroidal (vertical channels) or poloidal (horizontal channels) symmetry. The error on the measurement is ±10%.

The low gas puffing pulse, exhibits low ELM frequency and high bulk radiated power, close to the total input power. As the gas puffing is increased, the ELM frequency increases and the bulk radiated power is reduced, showing a decrease of the W concentration in the plasma core. However, the use of gas to increase the ELM frequency leads to the degradation of the plasma stored energy, in this example by ~1MJ.

The ELM frequency can also be increased by ELM triggering by fast vertical plasma movements (so-called ”vertical kicks”) [9] and by ELM pacing with pellets [20], where a pellet triggers an ELM without impacting the plasma density. The efficiency of vertical kicks

for triggering ELMs and therefore control W in the core, depends on the plasma parameters, kick size (amplitude of the plasma oscillation) as well as the values of the W concentration. For values of W concentration $> 10^{-5}$ the increase of ELM frequency by kicks does not avoid the slow accumulation of W and a radiative collapse of the plasma is observed. ELM frequency control by pellet pacing has been demonstrated at JET, but due to constrains on the pellet system, not much work has been done on this and it is expected that for the JET next campaigns the system will be available and used routinely to control the ELM frequency. ELM frequency does not only control the W influx as it can also affect the W source.

In order to understand W transport and the efficiency of the different methods to control the source and accumulation, it is crucial to have an accurate quantification of the W content in the plasma and of the W source.

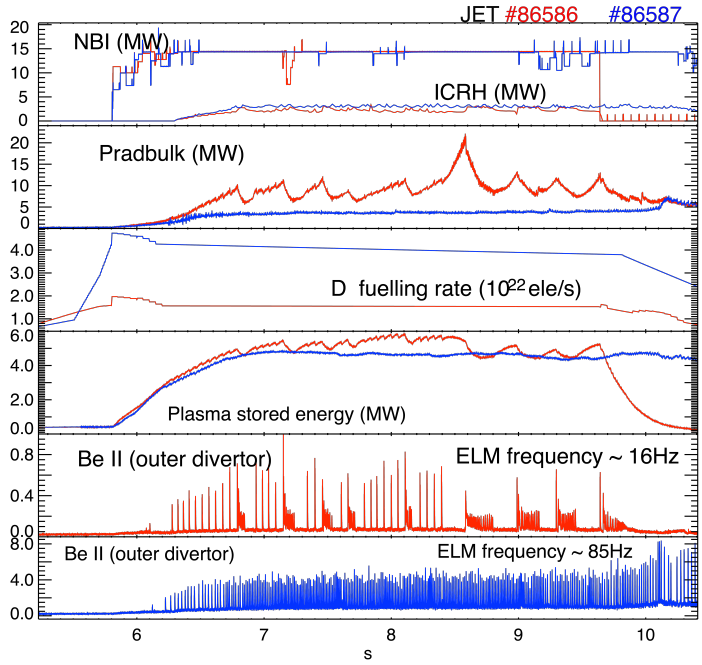

Figure 4 – Example of the effect of gas puffing on ELM frequency for the control of W accumulation. As the gas puffing increases, the ELM frequency increases and the bulk radiated power decreases. The plasma stored energy also decreases.

The total W content in the plasma is derived from the modelling of the signals from two soft X-ray cameras with Be filters and a spectrometer in the VUV range. The soft X-ray cameras allow for a detailed accounting of core radiation and poloidal asymmetries, the latter explained by parallel transport in the presence of centrifugal forces using rotation velocities consistent with charge-exchange recombination spectroscopy. To derive the absolute concentration, the Bremstrahlung contribution is removed and the excess radiation is attributed to W. The atomic data (from ADAS) is then used to interpret the excess radiation taking into account the Be filters and diode responses. On top of line radiation and radiative recombination a rough model for dielectronic recombination is included. To confirm that the SXR radiator was W, experiments injecting W into the plasmas by delaminating W source with a laser. Whilst the method above provides ELM averaged values, recently, a novel method based on the cross-calibration between a divertor spectrometer with a 40ms time resolution and a Photo Multiplier Tube measuring absolute photon fluxes with a 0.1ms temporal resolution. Both spectroscopic methods look at neutral W emission at 400.9 nm [21]. This method allows the quantification of W source information during and in-between ELMs for a wide range of ELMy H-mode plasmas with varying ELM frequency and plasma temperature at the divertor target above 10eV.

Figure 5 shows the total averaged W source and plasma average W content as a function of the ELM frequency determined by the application of this novel method for a wide range of type I ELMy H-modes. For all the pulses analised in this study, the ELM frequency is increased by increasing the gas puffing rate which also reduces the ELM size and increases the radiated power at the divertor. It is observed that the W source due to the ELMs increases linearly with the ELM frequency. Despite the increase of W source, the total W content in the

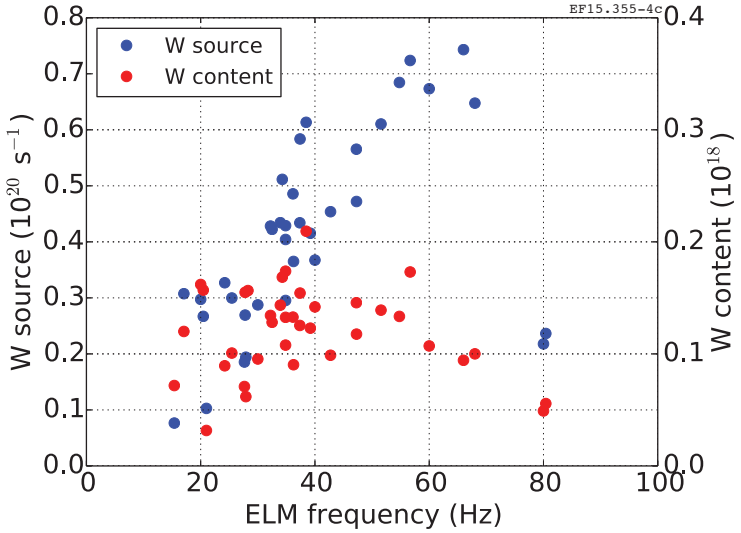

Figure 5 – Total W source and plasma total W content as a function of the ELM frequency for a wide range of ELMy H-mode plasmas. Figure from [21].

plasma decreases for ELM frequencies above ~50Hz indicating that the W flushing by ELMs dominates over the source and that the W confinement time depends on the ELM frequency $\tau_W \propto f_{ELM}^{-0.45}$ as reported in [22]. "Vertical kicks" were also used to impose the ELM frequency whilst maintaining the gas puffing rate constant. The results show that for attached plasmas and ELM frequencies up ~50Hz, the contribution of the gas puffing in the reduction of the W source is negligible.

3. Overview of global energy confinement of JET-ILW and JET-C plasmas

In order to predict the confinement performance of burning plasmas, a global scaling for energy confinement time (τ_E) or stored energy (W) has been derived empirically using engineering parameters, the so-called IPB98(y,2) scaling [23]:

$$\tau_{98(y,2)} = 0.0562 I_p^{0.93} B_t^{0.15} n_{19}^{0.41} P_L^{-0.69} R^{1.97} \varepsilon^{0.58} \kappa_a^{0.78} M^{0.19}$$

where I_p is the plasma current (MA), B_t the magnetic toroidal field (T), n is the plasma density, P_L is the loss power ($P_L \equiv P - dW/dt$), R is the major radius and a the minor radius with ε the inverse aspect ratio defined by a/R. M is the ion mass number and κ_a is the effective elongation defined by $\kappa_a = S_c/\pi a^2$, where S_c is the plasmas cross-sectional area and M the effective isotope mass, here M=2 for deuterium plasmas.
The predicted normalized plasma energy confinement ($H_{98(y,2)}$)is then defined by:

$$H_{98(y,2)} = \frac{W_{th}}{W_{98(y,2)}} = \frac{\tau_{measured}}{\tau_{98(y,2)}}$$

At the end of the JET-C campaigns, much progress had been achieved in understanding plasma energy confinement, its dependences and the physics processes involved, such as transport physics in the core, the edge and its connection, for a wide variety of plasma regimes and conditions. In JET-C, plasmas with high energy content up to 12MJ with conditions approaching those of a fusion reactor were achieved [24].

The development of high energy plasmas at JET is key to demonstrate the compatibility of high performance operation with a metallic wall mimicking ITER operation as well as the demonstration of high plasma confinement in the presence of impurities resulting from material sputtering which were not present in a carbon wall. The development of such high energy plasmas was performed in both JET-C and JET-ILW and the results compared as shown in figure 6 where $W_{th}$is plotted as a function of $W_{98}$for the scenarios with β_N~1.8-2 (so-called baseline scenario) and β_N>2.5 (so-called hybrid scenario). Initial results showed a degradation of the plasma stored energy for the baseline plasmas whilst for the hybrid

plasmas, the stored energy is similar to that obtained in JET-C [19]. This loss of plasma confinement at low β_N is mostly due to the loss of pedestal temperature as shown in figure 7 [25].

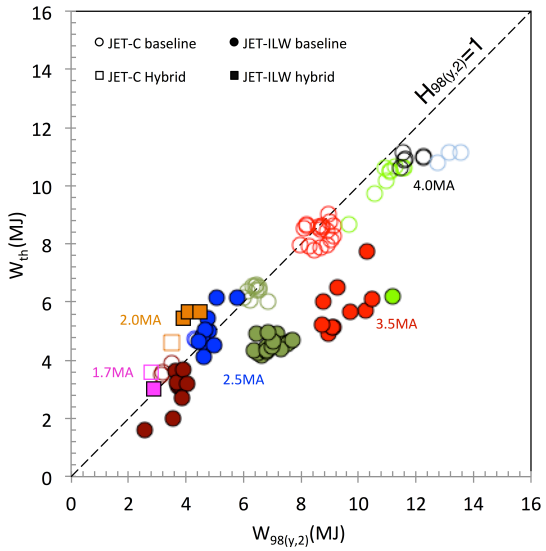

Figure 6 – JET-C: baseline (empty circles) with δ~0.25 and β_N~2.0 for Ip ≤ 4MA and β_N<1.8 for Ip>4MA and hybrid (empty squares) with β_N~2.9-3.2. JET-ILW baseline (full circles) with δ~0.25; β_N~1.8 for I_p≤2.5MA and β_N<1.6 for I_p>2.5MA. and hybrid with β_N~2.0-3.3.

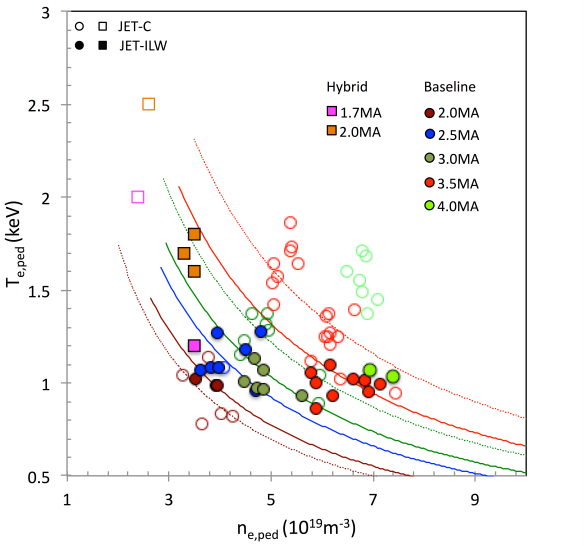

Figure 7 – Pedestal temperature and density diagram for JET-C baseline (open circles) and hybrid (open squares) discharges and JET-ILW baseline (full circles) and hybrids (full squares) discharges. The constant pressure lines for JET-C (continuous) and for JET-ILW (dashed) baseline scenario are also shown for discharges at 2.0, 2.5, 3.0, and 3.5MA (colours the same as for the circles). Currents above 4MA are not shown in this figure.

For the baseline scenario, plasmas with similar stored energy to those of JET-C plasmas have been achieved for plasma currents up to 2.5MA, but as the plasma current increases, the measured plasma energy is substantially lower than that of JET-C. This difference of the pedestal temperature is clearly illustrated in figure 7 where the density and temperature at the pedestal are shown for similar plasmas in JET-C and in JET-ILW. Here a strong decrease of the edge temperature leads to a strong decrease of the core temperature (due to stiffness). This reduction of the pedestal temperature in JET-ILW strongly impacts the pedestal pressure as shown in figure 7 by the constant pressure lines for discharges at different plasma currents and in table 1.

$P_{e,ped}$ (kPa)	**2.0MA**	**2.5MA**	**3.0MA**	**3.5MA**
CFC	5.57	7	9.8	13
ILW	6.2	7.4	8.3	10.6

Table 1: Pedestal pressure values for plasma discharges at the same plasma current and safety factor field.

Increasing the additional input power and reducing the gas puffing rate, gives access to high β_N (>2.5) plasmas with high pedestal temperature as shown in figure 7 (squares). In

these plasmas, the favourable power dependence of the pedestal confinement with β leads to an improved global confinement [26].

Another effect on plasma behaviour due to the change of the wall materials was the loss of confinement at high triangularity (δ>0.4) high density plasmas. In JET-C, at high triangularity low collisionality, plasmas with $H_{98(y,2)}$~1 could be achieved at densities close to the Greenwald density [27] due to a change in transport or pedestal stability, where mixed type I-II ELMs replaced the typical type I ELMs with increasing inter-ELM losses [28]. In the JET-ILW, high and low triangularity plasmas show similar behaviour at high and low density, and the mixed type I-II ELM regime has not yet been achieved. One common factor to these plasmas with low confinement is the plasmas low temperature, hence high collisionality. Recent studies show that JET-ILW low collisionality plasmas can reach confinement values comparable to those of JET-C [29] and that at similar collisionality the pedestal temperature and stored energy are similar.

4. Impact of JET-ILW on pedestal confinement

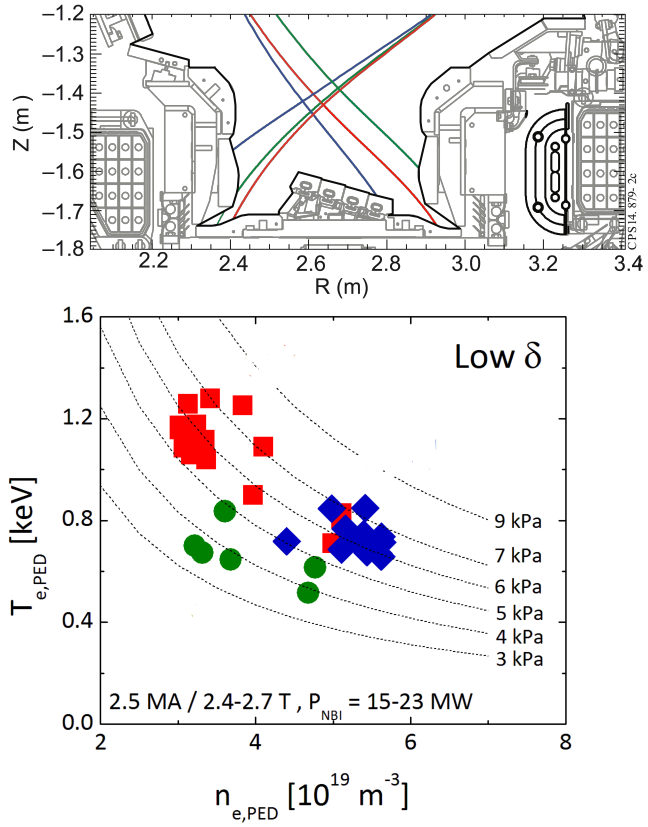

Figure 8 – Top: divertor geometries with outer strike points at different distances from pump throat at 3.0m. Bottom: Variation of $T_{e,ped}$ and $n_{e,ped}$ as function of divertor geometry. Figure from [37].

The observed effect of pumping efficiency on the pedestal confinement has highlighted the importance of the plasma-wall interaction physics in determining the plasma performance. With increasing pumping efficiency, an improvement of the pedestal confinement is observed as shown in figure 8. It is not clear if this effect is related to the change of neutrals and recycling in the main chamber or changes in the pedestal stability. However, the impact of particle source on plasma confinement is confirmed by its degradation as gas puffing is increased. In order to assess the changes on confinement as a consequence of pumping efficiency, an experiment was performed where the plasma configuration in the divertor was changed. Here it is observed that as the strike points move closer to the cryopump, therefore improving pumping, the pedestal density decreases leading to the rise of the pedestal temperature and increasing the pedestal confinement by ~20% [30, 31]. It is worth noting that this effect was already observed in JET-C although with much lower impact on the global confinement [32] and that in JET-C, the majority of the discharges were done with zero gas puffing. Analysis of the recycling pattern demonstrate large variations for the configurations above, but no clear correlation between confinement and recycling can be inferred.

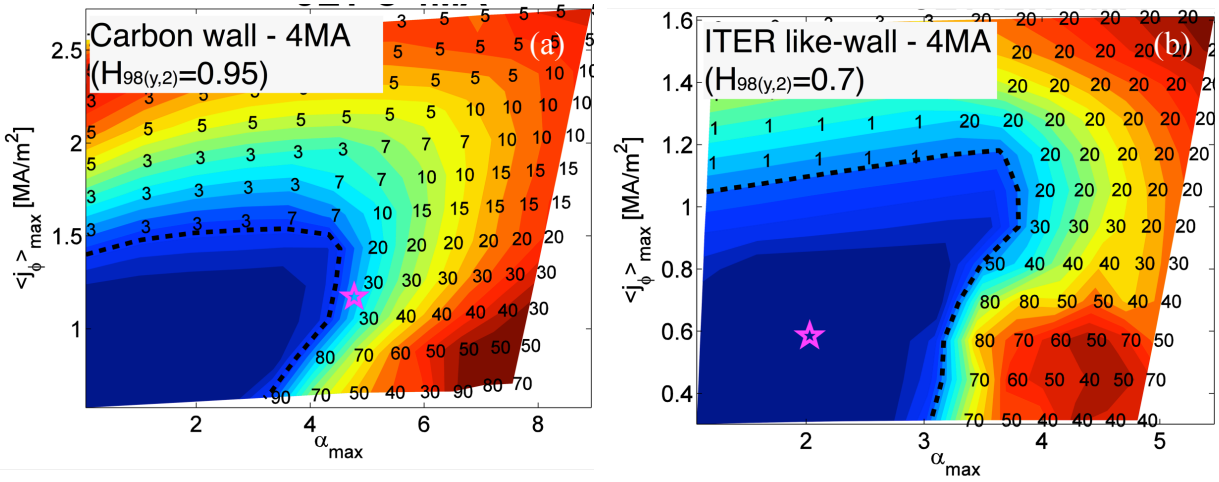

Figure 9 – Peeling-ballooning stability diagram for two 4MA pulses in (a) JET-C and (b) JET-ILW. The star represents the stability calculation of the plasma before the ELM occurs, the dashed line represents the P-B boundary between stable (blue) and unstable regions and the numbers represent the toroidal mode number. Figure from [38].

Simulations using SOLEDGE2D confirm that the total power losses inside the separatrix have a minimum for the configuration with higher pumping. However, these results are not conclusive as the amplitude of the power losses are too small relative to the total heating power, making it unlikely to be responsible for such large variations in confinement [32, 33].

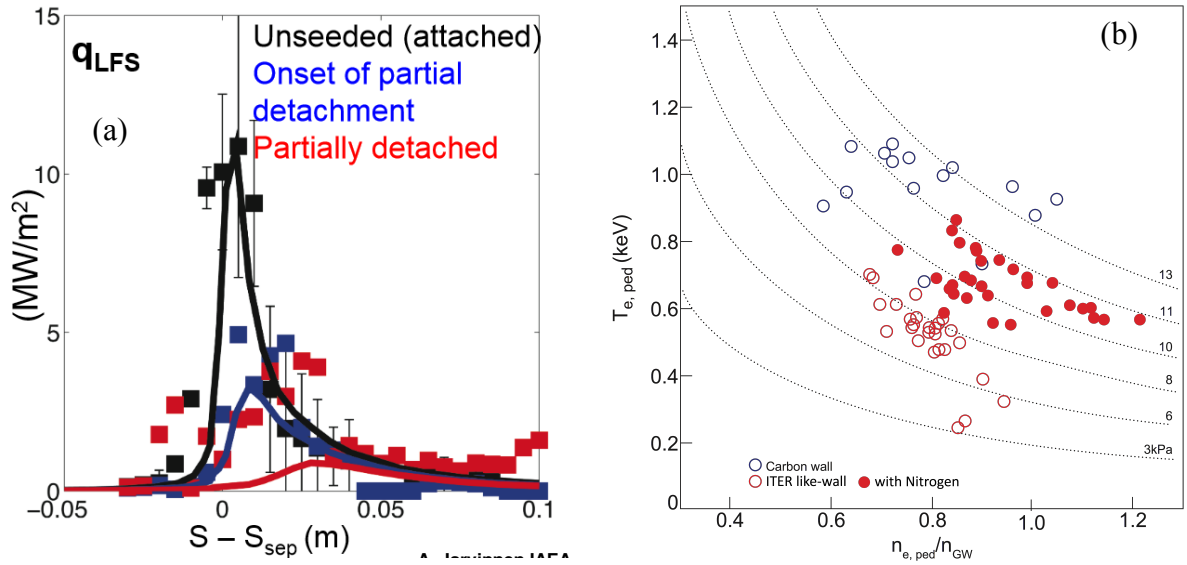

Figure 10 – (a) Comparison of experimental results (squares) and simulation results using 2D edge codes (line) of the radial distribution of power density without seeding (black) and increasing nitrogen levels to partial detached plasmas (blue to red). S-Ssep is the radial distance where zero is set at the plasma separatrix (S-Ssep=0). Figure from [39]. (b) Pedestal temperature as a function of the pedestal density normalized to the Greenwald fraction for carbon pulses (blue open circles), non-seeded (red open circles) and seeded (full red circles) JET-ILW discharges. Figure from [41].

Nevertheless, not all the impact on edge confinement can be explained by the change of recycling or neutrals. In JET-C and other devices [18, 34, 35], high triangularity plasmas showed good confinement at high density. Moreover, at JET a change in stability was also observed when the gas puffing rate was increased. Here, type I ELMs were replaced by mixed type I/type II ELMs with an increase of the inter-ELM transport. In the JET-ILW, this change

of pedestal stability at high triangularity is not observed even when the pumping efficiency is increased. The physics behind this change is not yet understood.

A stability analysis of the pedestal was performed for JET-ILW and JET-C low triangularity discharges at 2.5MA with similar confinement using the MISHKA and ELITE codes. The edge pressure in type I ELMy H-mode plasmas is constrained by ideal MHD peeling-balloning modes. When the stability limit is exceeded, the peeling–balloning mode is thought to cause an ELM crash, where the pedestal pressure is reduced. As shown in figure 9(a), for the JET-C discharge, the results are consistent with the Peeling-Balloning boundary [36, 37] i.e., ELMs are observed when the pedestal achieves a maximum pressure (α_{max}) defining the ballooning boundary and a critical edge current ($\langle j_\phi \rangle_{\max}$) defining the peeling boundary. For the low confinement discharges in JET-ILW, the results are not consistent with the P-B model. In this case, the P-B model estimates that the discharge is in the stable region i.e., no ELMs are predicted, whereas ELMs are observed experimentally. An example is shown in figure 9 for two 4.0MA discharges (a) from JET-C and (b) from JET-ILW [38]. These discharges are not similar in the sense that higher gas puffing is necessary for the 4MA discharge in JET-ILW in order to control the W accumulation which contributes to lower the plasma confinement. Both discharges have ICRH heating.

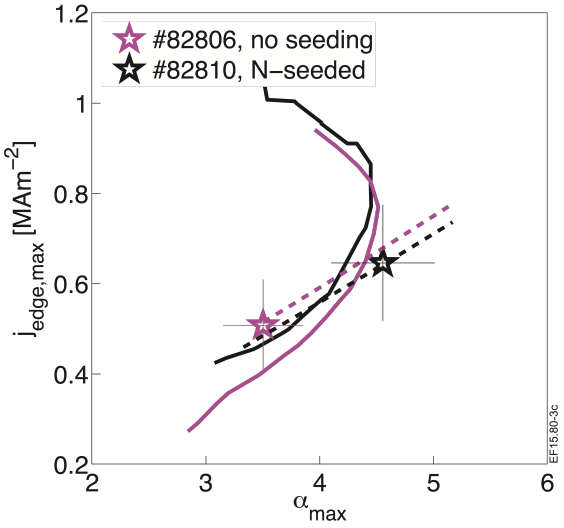

Figure 11 – P-B diagram for a seeded and unseeded discharge. For a similar P-B boundary, the discharge changes from the stable to the unstable region when seeding is added. Figure from [36].

Impurity seeding is used to increase the power dissipation in the divertor and reduce the W source. This induces partial (or full) detachment of the divertor by increased divertor radiation therefore reducing the plasma temperature close to the target plates. Figure 10(a) shows the radial distribution of the power density at the divertor for different levels of nitrogen seeding ranging from attached (no impurities), to partial or fully detached plasmas. The experiment is well reproduced by 2D edge codes [39]. Whilst similar behaviour in terms of detachment and ELM frequency is observed in both wall configurations, the effect of nitrogen seeding injection on the pedestal with a Be/W wall is the opposite from that of a carbon wall.

The injection of nitrogen has an opposite effect on plasma confinement for the JET-C and JET-ILW discharges; in JET-C the injection of nitrogen reduced the plasma global confinement whereas in the JET-ILW discharges an increase of the pedestal temperature leads to an increase of the global confinement as shown in figure 10(b). At high triangularity the confinement improves by ~30% whilst at low triangularity only a modest 10% increase is observed [40, 41]. It is not clear, if the change of radiation pattern at the edge is the responsible for the change of behaviour of the pedestal with nitrogen from the carbon wall to the Be/W wall. The radiation pattern of the nitrogen is similar to the radiation pattern of carbon, which might explain why by injecting nitrogen in an otherwise carbon free plasma part of the confinement is recovered. It is also possible that the nitrogen changes the edge turbulence, changing the transport properties at the edge. In nitrogen seeded plasmas, an increase of the pedestal pressure is observed due to both an increase of pedestal density and temperature. An analysis of the pedestal width and height shows that for increasing nitrogen

injection, the temperature width increases whilst the pedestal gradient slightly reduces. As the edge temperature increased, increasing the width without changing the gradient, indicates an increase of the pedestal height, which leads to higher pedestal pressures and higher edge current therefore better pedestal confinement. The pedestal stability analysis (figure 11) shows that in this case, the results are consistent with the P-B model whereas for the non-seeded case, the P-B model shows the discharge in the stable region. However, when neon is used as a gas to increase the power dissipation at the divertor target no effect on the plasma edge is observed [20, 41].

5. Impact of JET-ILW on core confinement

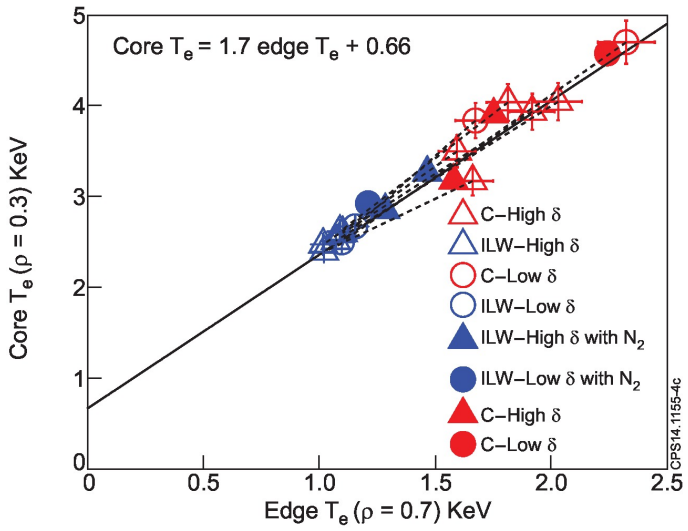

Figure 12 – Comparison of core and edge electron temperature for similar discharges performed with the Be/W and carbon CFCs. Figure from [42].

The change of the plasma facing components has changed significantly the plasma pedestal behaviour. The effect on the core confinement was assessed by doing a comparison of the transport analysis for unseeded JET-C discharges at both high and low triangularity and for seeded and unseeded JET-ILW discharges at high and low triangularity was performed as shown in figure 12 [42]. These results show that the core transport for the electrons is similar for both the JET-C and JET-ILW plasmas indicating that the core plasma behaves in a similar way to that with the carbon wall [43]. The increase of core pressure is due to the increase of density peaking and the increase of the ion temperature profile gradient as already observed in JET-C [44].

However, a change of the energy confinement time dependence with power (β_N) was observed [10]. A set of power scans were performed at constant plasma parameters where it was found that the power dependence of the energy confinement time is weaker than the IPB98(y,2) scaling for values of $\beta_N > 1.6$ for plasmas with low gas puffing (figure 13) whilst as the gas injection is increased, this dependence becomes stronger.

The improvement of the thermal stored energy with the heating power is due to a rise in both pedestal pressure, consistent with the P-B boundary, and core pressure peaking linked with the reduction of collisionality. Extensive linear and non-linear gyrokinetic simulations and linear magnetohydrodynamics (MHD) analyses have been performed in these discharges. These simulations show that under particular conditions at high input power, the large population of fast ions has a strong impact on core microturbulence and edge MHD by reducing core ion heat fluxes and increasing pedestal pressure in a feedback mechanism [45]. They also seem to indicate that the E × B flow shear has a minor effect but this effect is still being investigated.

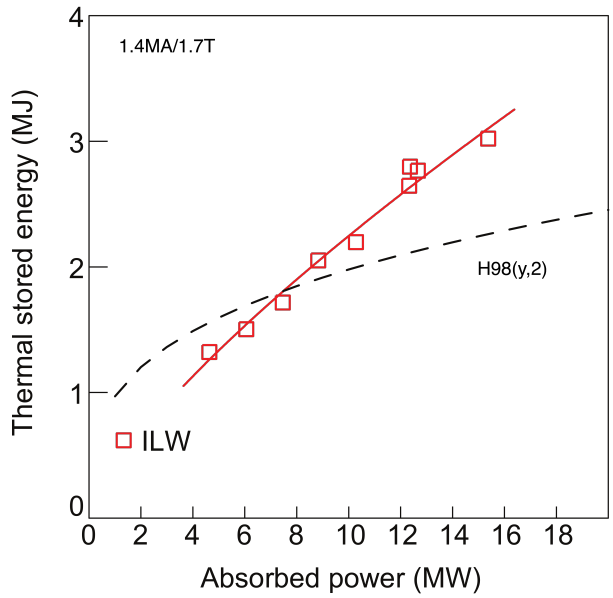

Figure 13- Dependence of the thermal stored energy for a power scan performed in the ITER-like wall compared with the IPB98(y,2) scaling. Figure from [10].

6. Summary

Operation at JET has changed with the new Be/W wall. W accumulation in the core and limitations on the power loads now need to be mitigated which has had an impact on the development of plasma scenarios relative to those with a carbon wall. The most striking effects on plasma behaviour resulting from the change of the plasma wall facing components were the reduction of pedestal temperature leading to the loss of plasma confinement and the change of edge stability. The change of edge stability is the most noticeable at high triangularity high density where good confinement was not yet achieved. This change on pedestal behaviour is not understood, and several hypothesis to explain this change were put forward, such as the change in recycling, the neutrals behaviour in the pedestal, as well as a change on edge stability due to the change of the wall material. It is also not clear what is the effect of the W at the edge and how much, if at all, contributes to the degradation of the pedestal. The W source and transport are well understood and ICRH and gas puffing are routinely used to control the W accumulation in the core whilst impurity seeding is used to control the W source. To achieve stationary plasmas, $f_{ELM} \gtrsim 30$Hz in order to control the W accumulation, which requires gas puffing. Nevertheless, as the scenario development progresses, plasmas with good confinement have been achieved and edge stability analysis shows a good agreement with the P-B model leading us to conclude that plasmas with good confinement are similar to those obtained with the carbon wall. In terms of the core confinement, it has been shown that both electron and ion stiffness are similar for both the carbon and Be/W wall. The use of extrinsic impurity seeding has deemed to be necessary in order to reduce the power loads to the divertor target. Nitrogen seeding showed to be beneficial not only for reducing the power load but an increase of the pedestal temperature was also observed and its effect is dependent on plasma triangularity. The mechanism that leads to the increase of pedestal temperature has not yet been identified (regarding nitrogen puffing). Overall, JET has demonstrated successful plasma operation with the beryllium/tungsten material combination, has confirmed its advantageous behaviour with respect to material migration and fuel retention and provided a strong scientific basis for the ITER material selection. The next step is to open the operational space to higher current high confinement in preparation for a deuterium/tritium (DT) campaign and to explore the higher auxiliary power available from NBI and ICRH and the new pellet system for a demonstration of compatibility of high performance plasmas with metallic wall with a DT mixture.

Ackowledgements
"*This work has been carried out within the framework of the EUROfusion Consortium and has received funding from the Euratom research and training programme 2014-2018 under grant agreement No 633053. The views and opinions expressed herein do not necessarily reflect those of the European Commission*."

[1] Phillips V. et al., Plasma Phys. Control. Fusion **42** (2000) B293 doi:10.1088/0741-3335/42/12B/322
[2] Pitts R, et al., J. Nucl. Mater. **415** (2011) S957 doi:10.1016/j.jnucmat.2011.01.114
[3] Brezinsek S et al., Nucl. Fusion **53** (2013) 083023 doi:10.1088/0029-5515/53/8/083023
[4] Brezinsek S. et al., Nucl. Fusion **55** (2015) 063021 doi:10.1088/0029-5515/55/6/063021
[5] Kallenbach A. et al., Plasma Phys. Control. Fusion **47** (2005) B207 doi:10.1088/0741-3335/47/12B/S16
[6] Dux R., et al., Nucl. Fusion, **51** (2011) 053002 doi:10.1088/0029-5515/51/5/053002
[7] Pueterich T. et al., Plasma Phys. Control. Fusion **55** (2013) 124036 doi:10.1088/0741-3335/55/12/124036
[8] Joffrin E. et al., Nucl. Fusion **54** (2014) 013011, doi:10.1088/0029-5515/54/1/013011
[9] de la Luna E. et al., Proc. 25th IAEA Fusion Energy Conference, St Petersburg (2014)
[10] Challis C., et al., Nucl. Fusion **55** (2015) 053031, doi:10.1088/0029-5515/55/5/053031
[11] Lerche E. et al., submitted to Nucl. Fusion
[12] Garbet, X. et al., Plasma Phys. Control. Fusion **46** (2004) B557 doi:10.1088/0741-3335/46/12B/045
[13] Angioni C. et al., Nucl. Fusion 44 (2004) 827 doi.org:10.1088/0029-5515/44/8/003
[14] Caason F. et al., Plasma Phys. Control. Fusion **57** (2015) 014031 doi:10.1088/0741-3335/57/1/014031
[15] Angioni C. et al., Nucl. Fusion **56** (2014) 124001 doi:10.1088/0741-3335/56/12/124001
[16] Angioni C. et al., Phys. of Plasmas **22** (2015) 055902 doi:10.1063/1.4919036
[17] Valisa M. et al., Proc. 25th IAEA Fusion Energy Conference, St. Petersburg (2014)
[18] Saibene G et al., Nuclear Fusion **39** (1999) 1133 doi:10.1088/0029-5515/39/9/307
[19] Beurskens M. et al., Plasma Phys. Control. Fusion **55** (2013) 124043, doi:10.1088/0741-3335/55/12/124043
[20] Lang P. et al., Nuclear Fusion **53** (2013) 073010 doi:10.1088/0029-5515/53/7/073010
[21] den Harder N. et al., submitted to Nucl. Fusion
[22] Fedorczak N. et al., Journal of Nucl. Mat. **463** (2014) doi:10.1016/j.jnucmat.2014.12.044
[23] ITER Physics Expert Groups on Confinement and Transport and Confinement Modelling and Database, ITER Physics Basis Editors and ITER EDA, Nucl. Fusion **39** (1999) 2175, doi:10.1088/0029-5515/39/12/302
[24] Nunes I. et al., Nucl. Fusion **53** (2013) 073020, doi:10.1088/0029-5515/53/7/073020
[25] Nunes I. et al., Proc. 25th IAEA Fusion Energy Conference, San Petersburg (2014)
[26] Challis C. et al., Nucl. Fusion 55 (2015) 053031 doi:10.1088/0029-5515/55/5/053031
[27] Greenwald M. et al., Plasma Phys. Control. Fusion **44** (2002) R27-R80
[28] Joffrin E., et al., Proc. 24th IAEA Fusion Energy Conference, San Diego (2012)
[29] Frassineti L. et al., Proc. 42nd European Physical Society, ECA Vol. 39E, P2-130, http://ocs.ciemat.es/EPS2015PAP/pdf/P2.130.pdf
[30] Tamain P. et al., 21st International Conference on Plasma Surface Interactions Kanazawa (2014)
[31] de la Luna E. et al., Proc. 25th IAEA Fusion Energy Conference, San Petersburg (2014)
[32] Groth M. et al., Nucl. Fusion **53** (2013) 093016 doi:10.1088/0029-5515/53/9/093016

[33] Bufferand H. et al., Journal Nucl. Mater. **438** (2013) S445 doi:10.1016/j.jnucmat.2013.01.090
[34] Stober J. et al., Plasma Phys. Control. Fusion **42** (2000) A211-215 doi:10.1088/0741-3335/42/5A/324
[35] Osborne T. et al., Plasma Phys. Control. Fusion **42** (2000) A175 doi:10.1088/0741-3335/42/5A/319
[36] Saarelma S. et al., Phys. of Plasma **22** (2015) 056115 doi:10.1063/1.4921413
[37] Maggi C. et al., submitted to Nucl. Fusion
[38] Stefanikova E. et al., Proc. 42nd European Physical Society, ECA Vol. 39E, P2-131, http://ocs.ciemat.es/EPS2015PAP/pdf/P2.131.pdf
[39] Jarvinen A. et al., Proc. 25th IAEA Fusion Energy Conference, San Petersburg, (2014)
[40] Maddison G. et al., Nucl. Fusion **54** (2014) 073016 doi:10.1088/0029-5515/54/7/073016
[41] Giroud C. et al., Plasma Phys. Control. Fusion 57 (2015) 035004 doi:10.1088/0741-3335/57/3/035004
[42] Kim H-T. et al., Plasma Phys. Control. Fusion **57** (2015) 065002 doi:10.1088/0741-3335/57/6/065002
[43] Tegnered D. et al., submitted to Plasma Phys. Control. Fusion
[44] Maslov M. et al., Nucl. Fusion **49** (2009) 075037 doi:10.1088/0029-5515/49/7/075037
[45] Garcia J. et al., Nucl. Fusion **55** (2015) 053007 doi:10.1088/0029-5515/55/5/053007